Applied Catalysis B: Environmental 185 (2016) 362–370

Contents lists available at ScienceDirect

Applied Catalysis B: Environmental

journal homepage: www.elsevier.com/locate/apcatb

# Zn-Cu promoted $TiO_2$ photocatalyst for $CO_2$ reduction with $H_2O$ under UV light

P.N. Paulino, V.M.M. Salim, N.S. Resende*

*Programa de Engenharia Química—COPPE, Universidade Federal do Rio de Janeiro, Centro de Tecnologia, Bloco G, sala 115 Cidade Universitária, P.O. Box 68502, 21941-914 Rio de Janeiro, RJ, Brazil*

ARTICLE INFO

*Article history:*
Received 9 June 2015
Received in revised form 8 December 2015
Accepted 18 December 2015
Available online 22 December 2015

*Keywords:*
Photoreduction
$CO_2$
Titanium dioxide
Copper oxide
Zinc oxide

ABSTRACT

The photocatalytic reduction of $CO_2$ has been studied aiming to find a useful application for such low cost and abundant raw material. Besides reducing $CO_2$ in the atmosphere, the process can contribute for the generation of high energy products ($CH_4$ and $CH_3OH$). The reaction was performed in liquid phase, batch, at 25 °C, with the photocatalyst (1 g/L) maintained in suspension. UVC lamp (18 W, 254 nm) was chosen as the radiation source. Photocatalysts were prepared using oxides of titanium, copper and zinc. Commercial $TiO_2$ (P-25, Degussa) was utilized as reference. Techniques such as $N_2$ adsorption, XRF, SEM-EDS, XRD, XPS, DRS UV–vis and TPD-$CO_2$ were used for photocatalysts characterization. Catalysts having specific area ranging from 36 to 52 $m^2/g$ and bandgap energies varying from 3.0 to 3.3 eV were obtained. TPD-$CO_2$ results showed different strengths of $CO_2$ adsorption for each photocatalyst. In the performance tests, $CH_4$ production achieved the range of 126–184 $\mu mol/g_{cat}$ after a 24 h-irradiation period. Regarding the photocatalysts tested, it was observed increased $CH_4$ formation in the following order: $TiO_2$ (P-25) ~ $TiO_2$ < 2%CuO/$TiO_2$ < 2%CuO–19%ZnO/$TiO_2$. Results indicate that the interaction between $CO_2$ and the photocatalyst influences the photocatalytic activity.



## 1. Introduction

As a consequence of new modes of production, since the Industrial Revolution, technology has had a profound effect on socioeconomic and environmental conditions. Atmospheric concentrations of $CO_2$ have grown exponentially since that period and nowadays it is considered the gas that mostly contributes to the greenhouse effect [1–3]. This assertion is questioned in numerous studies linking global warming to Earth's natural aging process and not to human activities. Even with those divergent views, there is a consensus toward the need to reduce $CO_2$ emissions.

Among the alternatives to decrease atmospheric $CO_2$ concentrations, $CO_2$ capture and sequestration is one of the most studied [4]. In this scenario, $CO_2$ reuse in chemical processes became an important issue and alternatives such as heterogeneous catalytic and electrocatalytic conversions were brought to light. The development of alternative production processes using $CO_2$ as a non-expensive feedstock or co-feeding may actually help to reduce the inconvenience caused by the uncontrolled release of gas.

The artificial photosynthesis process was named as such because of the similarity to nature's photosynthesis performed by plants [5,6]. While plants transform solar energy in chemical, with the help of chlorophyll, generating $O_2$ and glucose, $CO_2$ photocatalytic reduction is assisted by a photocatalyst and UV irradiation, transforming water and $CO_2$ into organic compounds of high energy level. Therefore, researchers dealing with artificial photosynthesis have great interest in environmental issues [7–9]. The choice for $CO_2$ photocatalytic reduction represents a sustainable and economically viable alternative: that is, it enables the use of both sunlight as a radiation source and $CO_2$ as raw material. The most employed photocatalysts in that type of reaction are semiconductor materials, such as $TiO_2$, ZnO and $ZrO_2$ [7,10–13].

Titanium dioxide ($TiO_2$) and zinc oxide (ZnO) are the most common materials used in heterogeneous photocatalysis for bringing the features of low cost, low toxicity, photostability, high catalytic activity [14], activation by sunlight and, finally, chemical stability over a wide pH range. The energy required to activate both oxides, $TiO_2$ and ZnO, by light is approximately 3.2 eV, which corresponds to UV radiation of wavelength shorter than 387 nm [15]. That characteristic enables the use of sunlight as the radiation source, since the wavelengths in this range represent approximately 3% of the solar spectrum that reaches the Earthís surface. Watanabe [16] has shown that ZnO can reduce $CO_2$ with a reductant molecule – $H_2O$

* Corresponding author.
*E-mail addresses:* priscillanpaulino@gmail.com (P.N. Paulino), neuman@peq.coppe.ufrj.br (N.S. Resende).

http://dx.doi.org/10.1016/j.apcatb.2015.12.037
0926-3373/

or $H_2$ – under high pressures of 25–35 kg/cm$^2$ of $CO_2$ gas generating oxygenated compounds. Pérez-Larios et al. [17] have used $TiO_2$–ZnO mixed oxides to improve from water splitting. The results showed an activity six times higher for $TiO_2$–ZnO-X mixed oxides than that for bare $TiO_2$ semiconductor.

Theoretical and experimental studies have shown that the crystal phase of $TiO_2$ and the defect disorders in $TiO_2$ have influence on $CO_2$ adsorption, activation and dissociation processes [13]. According to Rodriguez et al. [18], the presence of defects on $TiO_2$ surface induces the formation of new adsorption configurations, in which $CO_2$ is bonded at the defect sites. Electrons stored in the oxygen-deficient ($V_O$) can be spontaneously transferred to $CO_2$ and once the $CO_2^-$ is formed, the radical may decompose into CO through the occupation of one oxygen atom into the $V_O$ site.

Regarding photoreduction and photooxidation applications, the effect of metallic dopants, such as Ce, Cu, CuO, Pt, Au and Ag, in $TiO_2$ has also been reported [19,20]. However, a high concentration of metal/metal oxide can generate recombination centers of electron-hole pairs, leading to a reduction of photocatalytic efficiency. Another possibility is the use of nonmetals as doped and co-doped materials (for instance, C, N, S, F, etc.), which results in a significant narrowing of the bandgap, if compared to metal doping, leading to high photocatalytic efficiency under visible light irradiation [21–26].

Copper oxide (CuO) has been extensively studied in $CO_2$ photocatalytic reduction for several reasons. First, the presence of copper associated to the photocatalyst has an important role in $CH_3OH$ production, increasing significantly its production if compared to a photocatalyst without promoter. Another reason for using CuO is the redistribution of electric charge on the surface of the semiconductor support [10,19,27]. According to Tseng et al. [28], copper plays the role of a trapper of electrons preventing the recombination electron-hole pair and consequently promoting significant increase in photoefficiency. They have observed that the highest $CO_2$ conversion occurred when Cu content was 2% and that large amounts of photocatalyst in the reaction may hinder the diffusion of UV irradiation [28]. Slamet et al. [15] found that the photocatalysts promoted by CuO showed better performance than the materials promoted by the species $Cu^0$ and $Cu^{+1}$.

In the present study, the influence of Zn–Cu deposition on the photoactivity of $TiO_2$ has been investigated in the photocatalytic reduction of $CO_2$ with $H_2O$ to produce C1 fuels, such as $CH_4$ or $CH_3OH$. The direct impact of the presence of the brookite phase, instead of rutile phase, on the photocatalytic properties was also investigated. Additionally, $CO_2$ adsorption capacity of the photocatalysts was measured by temperature programmed $CO_2$ desorption to evaluate $CO_2$ interaction with the photocatalysts.

## 2. Experimental

### 2.1. Catalyst preparation

$TiO_2$ was prepared by slow hydrolysis of titanium isopropoxide—$Ti(OCH(CH_3)_2)_4$ (97%, SIGMA–ALDRICH). Due to the reagent instability, the reaction was carried out in inert atmosphere, using a plastic chamber previously filled with $N_2$. The precipitate obtained was filtered and washed, dried in an oven at 120 °C overnight and submitted to calcination at 550 °C for 6 h using airflow (30 mL/min) [29]. $TiO_2$ resulting from this procedure was used in the preparation of the other photocatalysts.

2%CuO/$TiO_2$ catalyst (CT) was prepared by the impregnation method employing $Cu(NO_3)_2{\cdot}3H_2O$ (99.5%, MERCK) to give the copper oxide. After impregnation, the material was dried in an oven at 120 °C for 24 h, and then, it underwent calcination at 500 °C for 3 h in the presence of air flow (30 mL/min).

2%CuO–19%ZnO/$TiO_2$ (CZT) was prepared by co-precipitation deposition method [30], using $Cu(NO_3)_2{\cdot}3H_2O$ (99.5%, MERCK), $Zn(NO_3)_2{\cdot}6H_2O$ (98%, VETEC) as precursor salts and a solution of 1 M $Na_2CO_3$ (99.5%, VETEC) as precipitation agent. The nominal content of copper and zinc oxides was 2% and 20% (%wt/wt), respectively. After co-precipitation, the material was filtered, washed and dried in an oven at 120 °C for 24 h and then subjected to calcination at 500 °C for 3 h in air flow (30 mL/min).

One of the most employed photocatalysts in related researches is the $TiO_2$ based photocatalyst (P-25) manufactured by Degussa, which has about 80% anatase crystalline phase and 20% rutile in its structure [7]. Thus, that material was used as reference for comparison with $TiO_2$ prepared in this study.

### 2.2. Catalyst characterization

Specific surface area (BET method), pore volume and average pore size (BJH method) of the samples were measured by $N_2$ adsorption analysis at −196 °C, using ASAP 2010 Micromeritics equipment. First, the samples were pretreated under vacuum at 300 °C for 12 h. After cooling, the volumetric method was used to proceed obtaining the isotherms.

The X-ray fluorescence (XRF) analysis was carried out in a RIX-3100 RIGAKU instrument, using Rh source, 50 kV and 80 mA. CT and CZT photocatalysts were analyzed in order to compare the oxide actual content to its nominal, and thus, detect possible impurities from the preparation methods.

A Miniflex TG RIGAKU instrument (Cu Kα = 1.54178 Å, 30 kV and 15 mA) was used for X-ray diffraction analysis. The step-scans were taken over the range of 2$\theta$ from 10° to 90° in steps of 0.05°, and the intensity data for each step was collected for 1 s. By analyzing the X-ray diffraction patterns, it was possible to identify the crystalline phases present in the material and the Fullproof software was used to quantify them.

Sample morphology was studied by a scanning electron microscope with field emission gun (FEG-SEM) (FEI Company, model QUANTA 400). In addition, elemental mappings were detected by an energy dispersive X-ray spectrometer (EDS) attached to the SEM.

The X-ray photoelectron spectra were obtained using Al Kα radiation with a Thermo Scientific (ESCALAB 250Xi), using C (1 s) as energy reference (284.6 eV).

UV–vis diffuse reflectance spectroscopy enabled the study of the UV absorption profile of the photocatalysts and the calculation of their energy bandgap. The spectra were obtained by a Cary 5 UV–vis-NIR (VARIAN) spectrometer, using $BaSO_4$ as reference. The reflectance spectra of the samples were analyzed under ambient conditions in the wavelength range of 200–800 nm. Reflectance was converted to $F(R)$ values using the Kubelka–Munk function Eq. (1):

$$F(R) = \frac{(1-R)^2}{2R} = \frac{k}{s} \quad (1)$$

where $R$ is the absolute reflectance, $k$ is the molar absorption coefficient and $s$ is the scattering coefficient. The bandgaps were obtained from the plot of $[F(R)\,h\upsilon]^{1/2}$ against the photon energy ($E$).

For the purpose of verifying the behavior of the photocatalysts in the presence of $CO_2$, all materials were analyzed by temperature programmed $CO_2$ desorption (TPD-$CO_2$). This technique enables to analyze the amount and types of sites that are present in the materials. To this end a multipurpose unit equipped with an online quadrupole mass detector QUADSTAR 422 (QMS 200, BALZERS) was used. First, the sample (100 mg) was placed into a quartz tube reactor, which was heated under ultra-high purity helium flow (60 mL/min) up to 200 °C at 10 °C/min for 1 h and then it was cooled to room temperature. After pretreatment, $CO_2$ flow (30 mL/min) passed through the catalyst bed for 30 min, subsequently the sam-

ple was flushed by He flow (60 mL/min) for 60 min. Then, the TPD analysis was performed under He flow (60 mL/min) by heating the sample at a rate of 20 °C/min up to 1000 °C. The effluent gases were monitored by online mass detector ($m/e$ = 2, 4, 28, 30, 32, 44 and 46).

### 2.3. Photocatalytic reaction

Photocatalytic reduction of $CO_2$ with $H_2O$ was conducted in liquid phase at a constant temperature of 25 °C and atmospheric pressure. The photocatalyst previously dried at 120 °C (concentration of 1 g/L) was suspended in 600 mL of 0.2 M NaOH. The alkaline solution was used for two reasons: to raise $CO_2$ solubility in the aqueous medium and to enhance the formation of •OH radicals [28]. Fig. 1 schematically illustrates the reaction unit.

The batch quartz reactor had an internal volume of 1180 mL (outer surface area of the reactor = 816.6 $cm^2$) and was illuminated by Hg vapor UVC lamp, low pressure (Puritec 18 W—254 nm, OSRAM) located in the center of the reactor. The gas inlet was made by a tube that went from the top to the bottom of the reactor. $CO_2$ with high purity (99.99%, LINDE) was used to avoid hydrocarbon contamination. Before turning on the lamp, $CO_2$ was bubbled at constant flow (100 mL/min) through the suspension during 40 min to clean the environment and saturate the solution. To avoid photocatalyst sedimentation, a magnetic stirrer was employed. A cooling bath (Proline PR 854, LAUDA) was used to maintain a constant temperature in the reaction medium. Temperature and pH were continuously monitored and measured by Schott pH meter (ProLab 2000, SCHOTT). The flux of the absorbed photons was measured by International Light Technologies radiometer (ILT1700) and calculated according to Tseng et al. [28].

Samples of the gaseous and liquid phases were taken regularly throughout the 28 h-process in order to monitor the reaction. Aliquots of 1 mL of the suspension were analyzed using a gas chromatograph (CP-3380, Varian), equipped with thermal conductivity and flame ionization detectors, employing a Poraplot-Q column. The gas samples were analyzed on a gas chromatograph (CP-3800, Varian) equipped with a methanetor, thermal conductivity and flame ionization detectors, using Molsieve 5 Å and Porabond columns.

Blank tests both, without UV irradiation and in the absence of $CO_2$ reagent were performed to certify that all products were generated from the photocatalytic reduction of $CO_2$ with $H_2O$.

Quantum yield of the $CO_2$ photoconversion (24 h reaction) can be calculated by Eqs. (2) and (3). Two and eight electrons are required to convert $CO_2$ to CO and $CH_4$, respectively [27].

$$\Phi_{CH_4}(\%) = \frac{8 \times \text{mol of} CH_4 \text{ formation}}{\text{mol of photons absorbed by photocatalyst}} \times 100\% \quad (2)$$

$$\Phi_{CO}(\%) = \frac{2 \times \text{mol of CO formation}}{\text{mol of photons absorbed by photocatalyst}} \times 100\% \quad (3)$$

The number of moles of photons absorbed by photocatalyst (MPAP) during 24 h was calculated by Eq. (4) and was approximately 125.5 mmol.

$$\text{MPAP} = \frac{\text{absorbed photon flux}(\mu W/cm^2) \times \text{outer surface area of reactor}(cm^2) \times \text{radiation time(s)}}{\text{each photon energy(J)} \times (6.02 \times 10^{23})} \quad (4)$$

## 3. Results and discussion

### 3.1. Photocatalysts characterization

XRD pattern of photocatalysts in Fig. 2 shows the anatase and brookite phases of $TiO_2$ with peaks of greater intensity in $2\theta = 25.28°$ and $2\theta = 25.34°$, respectively. As those peaks overlap, brookite phase identification was made by the second highest peak intensity at $2\theta = 30.81°$. The quantification of crystalline phases was estimated as 79% of anatase and 21% of brookite phases.

Regarding CT photocatalyst, no characteristic peak of either copper oxide ($2\theta = 35.5°$ and 36.4° for CuO and $Cu_2O$, respectively) or metallic copper ($2\theta = 43.3°$) was detected. This result is in agreement with a previous report on Cu content below 5% [8]. As well as the anatase and brookite phases, characteristic peaks corresponding to zincite phase (ZnO, $2\theta = 31.77°$, 36.25°, 56.60°, 67.96°) were also identified on CZT patterns.

In order to investigate the role of the impregnation of CuO in the structure of the starting material, the surface morphologies of those samples were analyzed by scanning electron microscopy (FEG-SEM) with energy dispersive X-rays detector (EDS). Fig. 3 presents SEM micrographs. Images (a) and (b) shows that the photocatalysts have a homogeneous surface with flocculated appearance. Similarity of images (a) and (b) confirms that the addition of CuO on $TiO_2$ did not modify the surface of the starting material. By analyzing CZT results (Fig. 3(c)), a formation of filamentous structures on $TiO_2$ was noticed.

Figs. 4 and 5 show the surface analysis from EDS on CT and CZT samples, respectively. Those analyses confirm the XRD results, indicating that CuO is well dispersed on $TiO_2$ surface in both photocatalysts. Regarding ZnO, EDS indicates a homogeneous dispersion all over the study area. The formation of crystals modified the surface but did not cause a total covering of $TiO_2$.

The chemical composition from XRF and the basic textural characterizations of the samples are summarized in Table 1, as well as the phases identified by XRD. The specific surface area ($S_{BET}$) of $TiO_2$ was 52 $m^2/g_{cat}$, which is consistent with the values (50–80 $m^2/g_{cat}$) found in previous reports [15,31,32]. The $S_{BET}$ value of CT, 36 $m^2/g_{cat}$, presented a decrease in relation to $TiO_2$, also consistent with the literature [33]. In relation to CZT sample, it is important to point out that the co-precipitation method used in that preparation has probably prevented a major decrease [34] on the specific surface area value found of 43 $m^2/g_{cat}$.

Table 1 summarizes the properties of the photocatalysts. XRF results show that the content of each oxide in CT and CZT samples is compatible with the nominal content, indicating no significant material loss in the preparation stages. The difference observed between Cu/Ti and Zn/Ti atomic ratios estimated from XPS and EDS analyses for the CZT photocatalyst shows the increasing concentration of Cu and Zn on the support ($TiO_2$) surface.

XPS spectra of the Cu photocatalysts are seen in Fig. 6. The respective binding energies of Ti $2p_{3/2}$ and Ti $2p_{1/2}$ (not shown) were found to be 458.1 and 463.8 eV, assigned to typical $Ti^{4+}$ [35]. Cu $2p_{3/2}$ and Cu $2p_{1/2}$ spin orbital splitting photoelectrons at binding energies of 932.8 and 952.8 eV, respectively were assigned to the compound $Cu_2O$ [36]. However, the major characteristic of $Cu^{2+}$ is the presence of the shake-up peak at 941.8 eV [37,38]. Therefore, XPS analyses of Cu 2p indicate that $Cu^{2+}$ and $Cu^{+}$ species coexist in both samples. The quantitative analyses showed that CT sample contains 54% $Cu^{1+}$ and 46% $Cu^{2+}$, while CZT has 51% $Cu^{1+}$ and 49% $Cu^{2+}$. The peaks characteristics of $Zn^{2+}$, Zn $2p_{3/2}$ and Zn $2p_{1/2}$ were found centered at 1021.7 and 1044.8 eV, respectively, [39].

DRS patterns of the photocatalysts are presented in Fig. 7. $TiO_2$ spectrum shows an absorption band with maximum around 350 nm associated to the process of charge transferring, $O^{2-}$ (2p) → $Ti^{4+}$ (3d) [9].

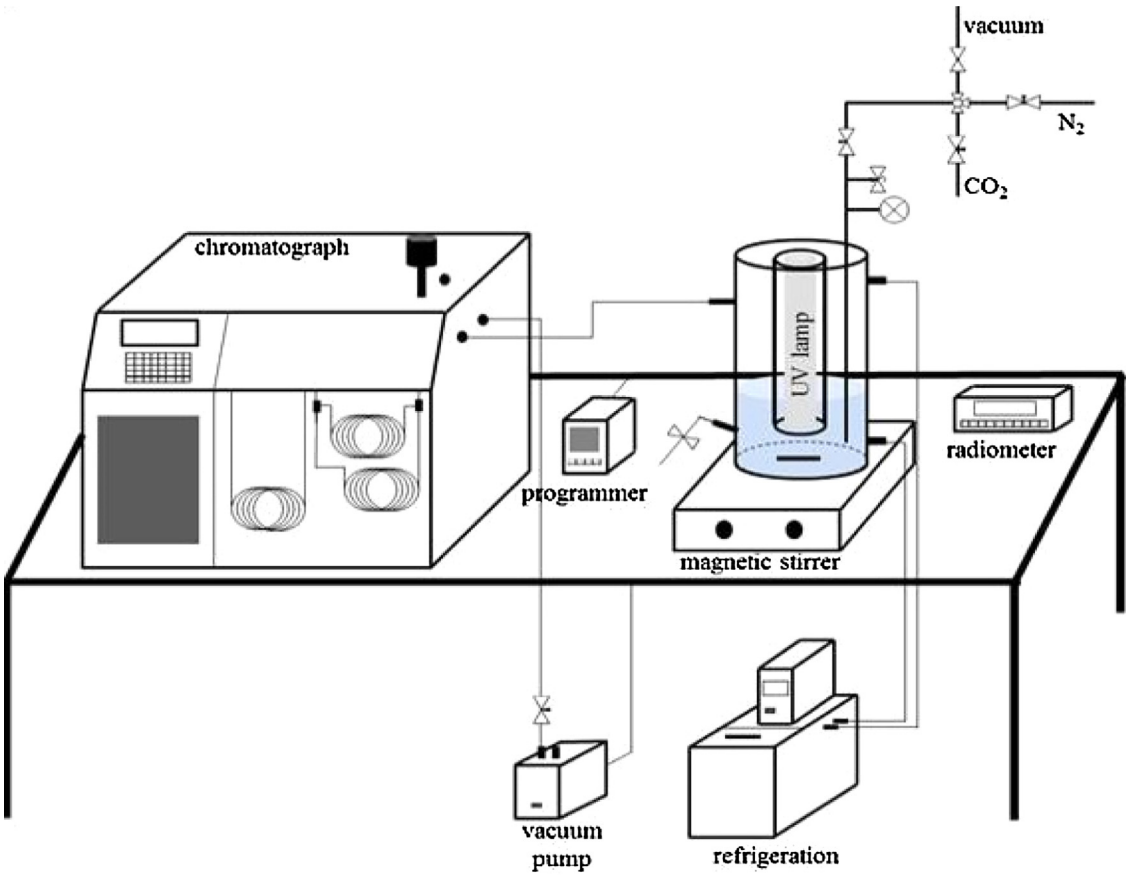


**Fig. 1.** Experimental setup of the photocatalytic unit.

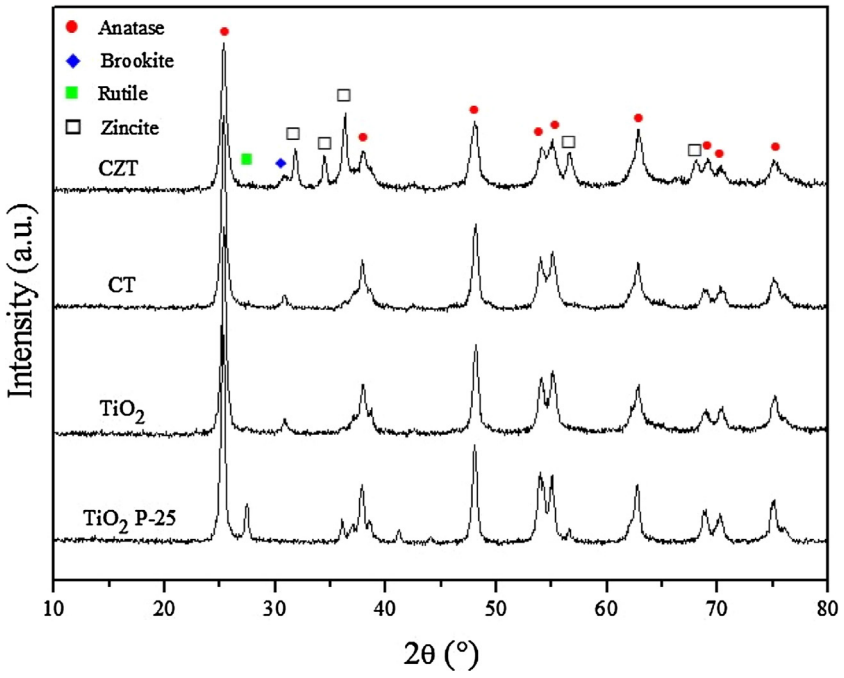


**Fig. 2.** XRD patterns of the photocatalysts.

The surface modification of $TiO_2$ using CuO and ZnO affected the absorption properties of the catalysts. When CuO was added, the $TiO_2$ photocatalyst absorbed the energy in the visible range around 380–500 nm. According to the literature [40], the band at 210–270 nm is attributed to the ligand-to-metal charge transfer transition of $O^{2-}$ (2p) → $Cu^{2+}$ (3d), occurring in isolated $Cu^{2+}$ sites. Additionally, the presence of $(Cu–O–Cu)^{2+}$ clusters highly dispersed is indicated by the band at 350 nm. In relation to ZnO, the energy

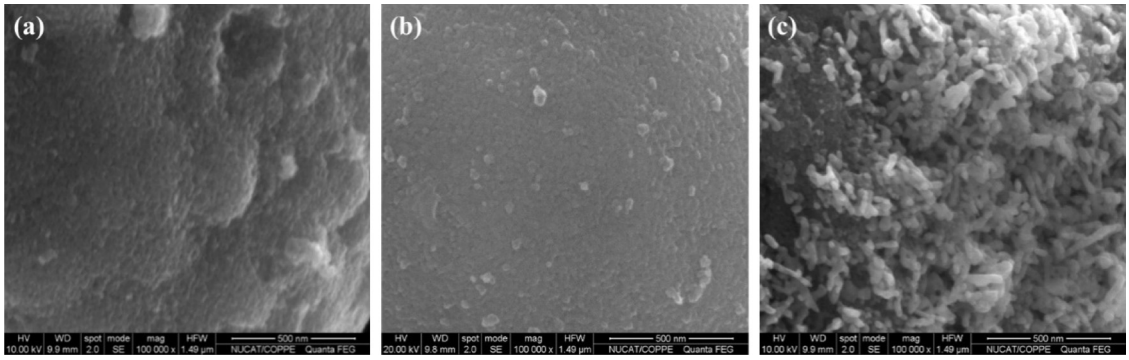


**Fig. 3.** SEM microphotographs of photocatalysts (a) $TiO_2$, (b) CT, (c) CZT.

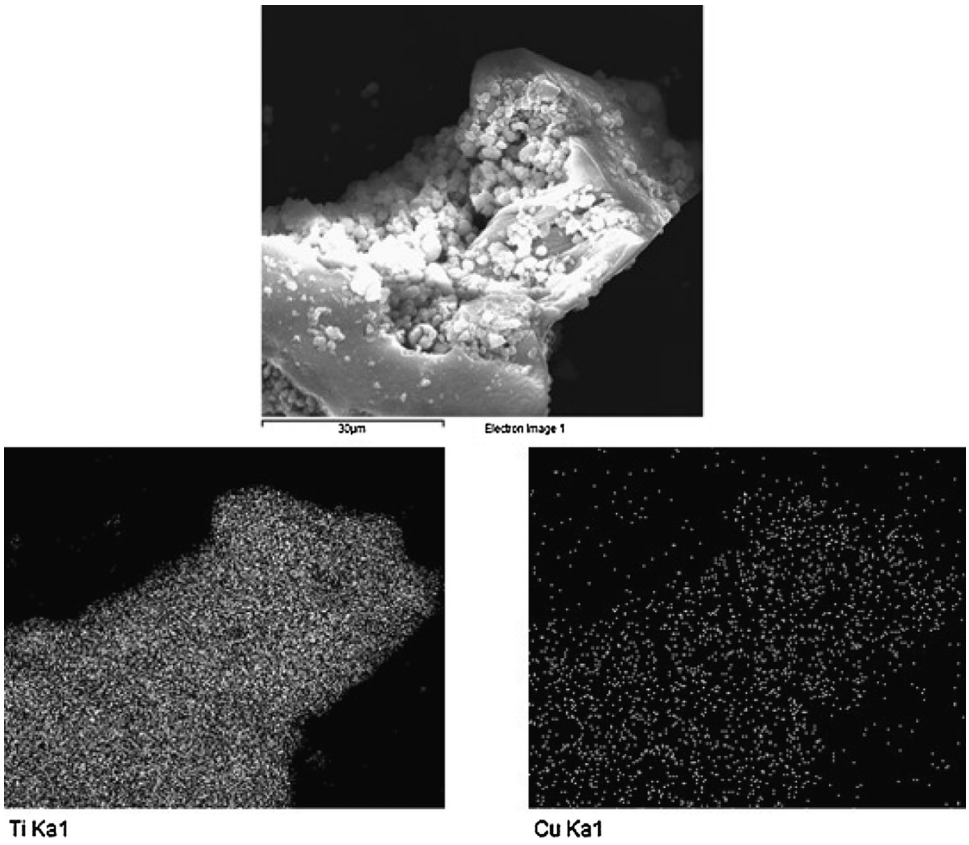


**Fig. 4.** SEM image and elemental mapping of CT.

**Table 1**
Chemical composition (XRF), structural (XRD) and textural characterization of photocatalyst samples.

| Catalyst | Content (%wt)[a] | | $S_{BET}$ | Pore volume | $d$ | Identified phases[b] | | Atomic ratio | | | |
|---|---|---|---|---|---|---|---|---|---|---|---|
| | | | | | | XPS[c] | | EDS[d] | | | |
| | CuO | ZnO | ($m^2$/g) | ($cm^3$/g) | (Å) | $TiO_2$ | ZnO | Cu/Ti | Zn/Ti | Cu/Ti | Zn/Ti |
| $TiO_2$ P-25 | – | – | 49 | – | – | A + R | – | – | – | – | – |
| $TiO_2$ | – | – | 52 | 0.14 | 108 | A + B | – | – | – | – | – |
| CT | 2.4 | – | 36 | 0.12 | 124 | A + B | – | 0.12 | – | 0.03 | – |
| CZT | 2.2 | 19.2 | 43 | 0.15 | 126 | A + B | Z | 0.3 | 4.12 | 0.03 | 0.22 |

[a] Estimated from XRF.
[b] Estimated from XRD. A: anatase; B: brookite; R: rutile; Z: zincite.
[c] Superficial.
[d] Near bulk [28].

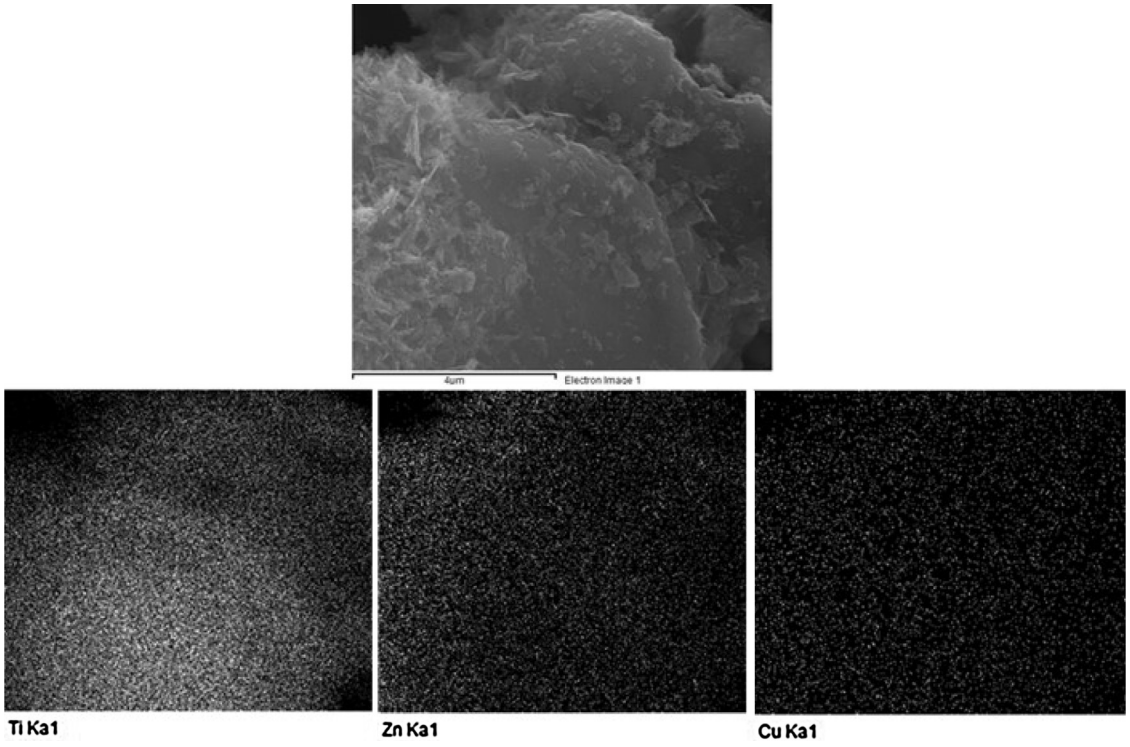


**Fig. 5.** SEM image and elemental mapping of CZT.

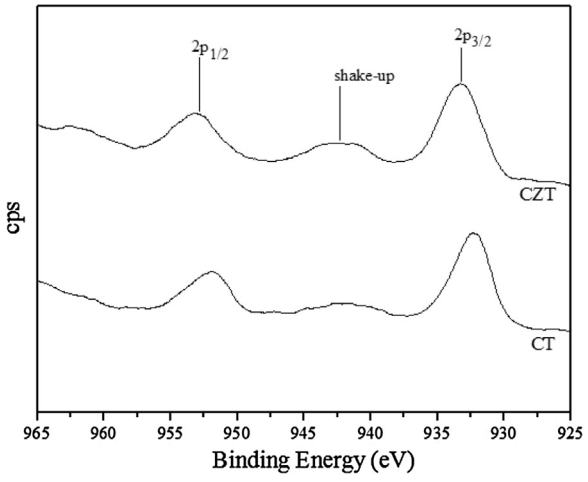


**Fig. 6.** XPS spectra of Cu 2p of CT and CZT photocatalysts.

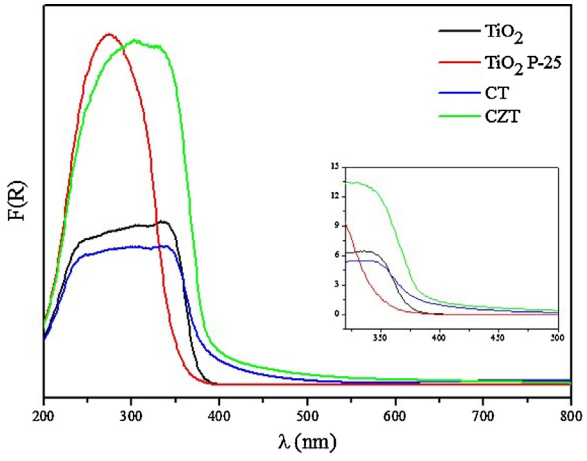


**Fig. 7.** DRS patterns of UV–vis photocatalysts.

absorption spectrum presents a wavelength absorption maximum near to 400 nm similar to $TiO_2$ [41]. CZT photocatalyst spectrum presented a wider band than the spectra of the other photocatalysts, suggesting higher photocatalytic activity.

$TiO_2$ prepared in this study has shown similar bandgap energy to commercial $TiO_2$ (P-25). However, the addition of copper and zinc oxides to $TiO_2$ has provided a decrease in its original value. CT photocatalyst presented a bandgap of 2.95 eV which is corroborated by literature [15]. The bandgap change indicates that the insertion of copper oxide modified the material, causing a redistribution of its electrical charge. Copper acts as a hole scavenger resulting in a longer separation between the electron-hole pairs generated by increasing material photoefficiency. Slamet et al. [15] observed that the bandgap value is inversely proportional to CuO content in the photocatalyst. They achieved values of about 3.05 and 2.88 eV for 0.5%CuO/$TiO_2$ and 3.0%CuO/$TiO_2$, respectively. As it was expected, ZnO did not promote a decrease of the bandgap energy for CZT photocatalyst since its bandgap value is similar to that of $TiO_2$ [42]. The bandgap values shown in Table 2 were estimated by extrapolation of the linear part of the DRS spectrum in Fig. 8 [31].

**Table 2**
$CO_2$ adsorption capacities and bandgap energies for the photocatalysts.

| Photocatalyst | Bandgap (eV) | $q_{max}$ $CO_2$ (μmol/g) |
|---|---|---|
| $TiO_2$ (P-25) | 3.25 | 59.4 ± 5.3 |
| $TiO_2$ | 3.17 | 10.2 ± 0.9 |
| CT | 2.95 | 36.2 ± 3.3 |
| CZT | 3.02 | 227.7 ± 20.5 |

TPD-$CO_2$ profiles obtained for all photocatalysts are presented in Fig. 9. The desorbed $CO_2$ amount was determined by the measurements/integration of signal $m/e = 44$ area and corrected by the gas sensitivity factor obtained by injection pulses of a known amount

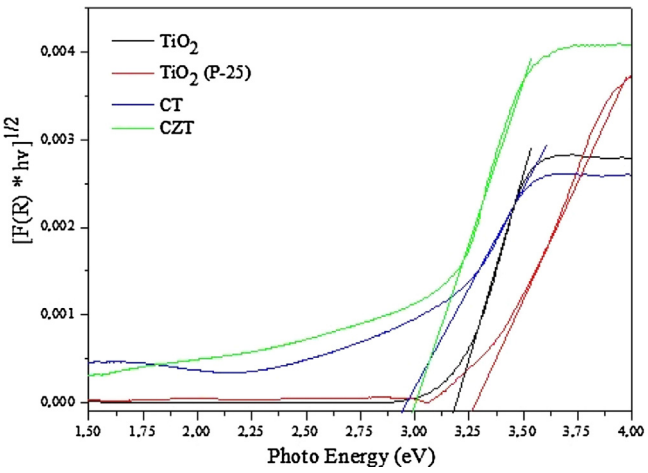


**Fig. 8.** Determination of bandgap from DRS spectra.

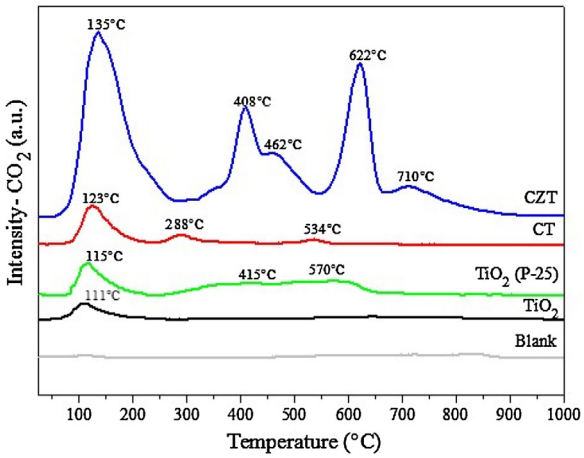


**Fig. 9.** TPD-$CO_2$ profiles for $TiO_2$ based photocatalysts.

of gas. The amount of $CO_2$ desorbed ($q_{max}$ $CO_2$) by photocatalysts are presented in Table 2.

The profiles of $TiO_2$ and $TiO_2$ (P-25) show $CO_2$ desorption at low temperature, with $T_{max}$ equal to 111 °C and 115 °C, respectively, indicating low interaction between $CO_2$ and the photocatalyst. However, this interaction is probably higher for $TiO_2$ P-25 due to the desorption range between 300 °C and 600 °C. CT and CZT profiles show a modification of $CO_2$ adsorption sites. They present higher desorption peak at temperatures 123, 288, 534 °C and 135, 408, 462, 622 and 710 °C, respectively. CZT has chemisorbed a more expressive amount of $CO_2$ than the other materials, indicating an increase in the photocatalyst affinity. Nevertheless, the alkalinity due to ZnO addition has also contributed to the increase of $CO_2$ adsorption capacity [43].

On the basis of our experimental results, some considerations should be pointed out. $TiO_2$ prepared in this study presented a different crystalline phase than the reference ($TiO_2$ P-25, Degussa). This result enables an assessment of the brookite phase photoactivity in the studied reaction. CuO and ZnO are dispersed on the surface of their respective photocatalysts. These oxides could play a role in the inhibition of the deactivation by recombination of hole-electron pairs. Bandgap values suggest that CZT photocatalyst will present enhanced photocatalytic activity. The samples have exhibited different affinities of $CO_2$-photocatalyst which could be assessed in the photocatalytic reduction of $CO_2$ with water. The characterization results suggest that CZT photocatalyst can present a better photocatalytic activity compared to that of $TiO_2$ and CT due to higher probability of obtaining the radical $CO_2$.

### 3.2. $CO_2$ photocatalytic reaction

All blank tests presented no products or precipitate in aqueous medium. The analysis of gas samples indicated the formation of $CH_4$ and CO as the only products of $CO_2$ photoreduction reaction. Liquid phase analysis showed no products.

Increasing formation of $CH_4$ was observed during the 28 h of continuous irradiation as shown in Fig. 10. CO presented a different behavior reaching maximum concentration after around 6 h of test which gradually decreased afterwards. This behavior may be a strong indication that CO is an intermediate of $CH_4$ formation in $CO_2$ photocatalytic reduction, as suggested by several researchers [7,31].

$CH_4$ formation increased during the tests with all the photocatalysts, in the following order: $TiO_2$ (P-25) ~ $TiO_2$ < CT < CZT, and total $CH_4$ production in 24 h was 126, 128, 153 and 184 μmol/$g_{cat}$, respectively. The highest $CH_4$ formation exhibited by CZT photocatalyst confirms the prediction by DRS UV–vis results that this sample should show the best photoactivity.

$CH_4$ formation for both $TiO_2$, prepared and commercial (P-25, Degussa), was nearly the same, meaning similar photocatalytic activity. This is a great result, taking into account that the composition (anatase and rutile) of commercial $TiO_2$ (P-25) is considered a reference in photoreactions. It is noteworthy that $TiO_2$ photocatalyst prepared by slow hydrolysis of titanium isopropyl oxide resulted in a material containing 79% anatase phase and 21% brookite phase. While several researchers have investigated the photocatalytic ability of anatase-rutile, only few studies have employed brookite phase [44]. Due to the lack of studies up to this moment, the brookite phase has always been considered a less photoactive crystalline structure [45]. The results shown in the present study have evidenced that deeper investigations should be conducted on brookite photoactivity and also on the combination of anatase and brookite phases.

Table 3 shows the results for $CH_4$ and $CH_3OH$ formation obtained in the literature. It is important to point out that those values were obtained employing different methodologies, including the analysis of the reaction medium—gas or liquid. According to Tseng et al. [28], product formation in the photocatalytic reduction of $CO_2$ can be substantially modified by the reaction conditions, such as: UV intensity, UV wavelength, additives of reaction media and reactor configuration. Our results of the analysis of the liquid phase, show no formation of $CH_3OH$, which can be explained by the presence of both cations, $Cu^{1+}$ and $Cu^{2+}$, in the surface of the photocatalysts CT and CZT, as showed by XPS results. Many studies have discussed the role of these cations in the production of $CH_3OH$ in this reaction [10,27]. Slamet et al. [15] studied the influence of $Cu^0$, $Cu^{1+}$ and $Cu^{2+}$ in $CH_3OH$ formation. Those authors noted that CuO is the most active dopant when compared with the other species, but they did not verify the coexistence of more than one promoter in the photocatalysts. Therefore, the presence of $Cu^{1+}$ and $Cu^{2+}$ species in CT and CZT photocatalysts could not have favored the formation of $CH_3OH$.

In relation to TPD-$CO_2$ analysis, it could also be asserted that $CO_2$ affinity for the photocatalyst is a highly influential factor in the studied reaction. Some variables of photocatalysis have already been investigated such as: intensity and maximum spectral wavelengths of the UV source [21,31,50,51]; however, $CO_2$-photocatalyst interaction has not been pointed out yet as an important variable in the $CO_2$ photocatalytic reduction with $H_2O$. Liu et al. [52], using in situ diffuse reflectance infrared fourier transform spectroscopy have demonstrated that $CO_2$-species are spontaneously dissociated into CO even in

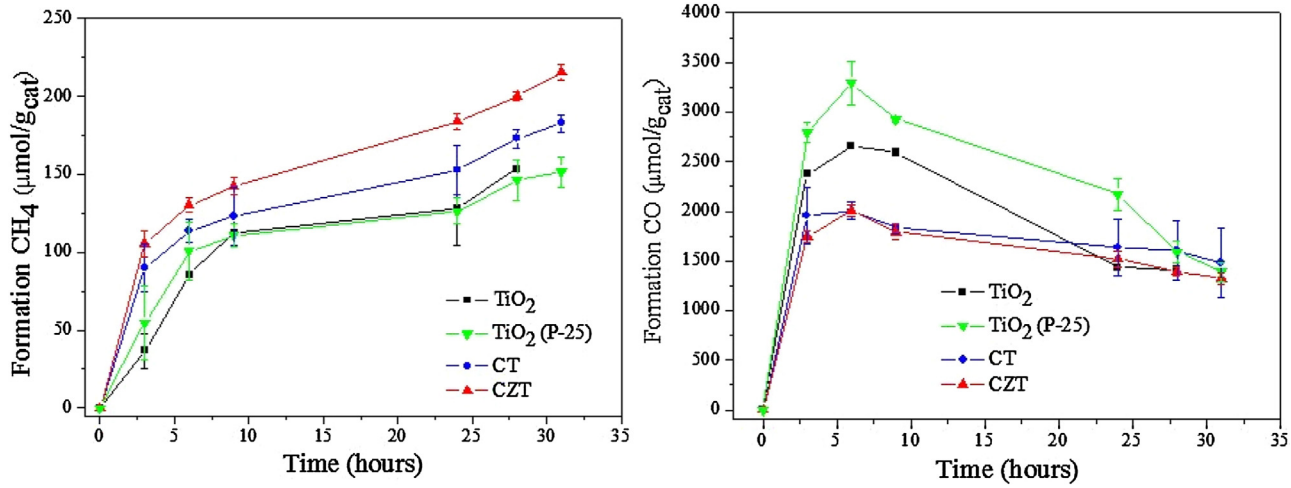


**Fig. 10.** Time dependence of product formation—$CH_4$ and CO.

**Table 3**
Comparison of products obtained after 24 h of photoreaction.

| Photocatalyst[a] | $CH_4$ (μmol/$g_{cat}$) | $CH_3OH$ (μmol/$g_{cat}$) | Reference |
|---|---|---|---|
| $TiO_2$ | 128 | – | This study |
| 2%CuO—CT | 153 | – | |
| 2%CuO–19%ZnO/$TiO_2$—CZT | 184 | – | |
| 2%Cu/$TiO_2$ | – | 500 | Tseng et al. [36] |
| 2%Cu/$TiO_2$ | – | 250 | Tseng et al. [28] |
| $TiO_2$ P-25 | – | 151.6 | Richardson |
| Cu/$TiO_2$ | – | 172.0 | et al. [46] |
| $TiO_2$–$ZrO_2$ | 15.5 | – | Matějová |
| Au/$TiO_2$ | 3.5 | – | et al. [47] |
| Pd(2%)–$TiO_2$ | 0.45 | – | Yui et al. [48] |
| 0.15 Pt/$TiO_2$NT | 115 | – | Zhang et al. |
| 0.12 Pt/$TiO_2$NP | 94 | – | [49] |
| $TiO_2$ NP | 9.5 | 1.5 | Kočí et al. [31] |
| $TiO_2/SO_4^{2-}$ | 18 | – | Lo et al. [50] |

[a] A: anatase; R: rutile; B: brookite; NT: nanotube, NP: nanoparticle.

the dark on partially oxygen depleted Cu(I)/TiO nanoparticles. They confirmed that the CO produced was derived from $CO_2$. Moreover, the surface $Cu^+$ species may facilitate destabilizing adsorbed $CO_2-$ and enhance its subsequent dissociation into CO.

The use of NaOH solution enabled a major $CO_2$ concentration in aqueous medium. Species such as $HCO_3^-$ and $CO_3^{2-}$ were involved in this type of reaction and the equilibrium is represented in Eqs. (6) and (7) [53]:

$$CO_2 + H_2O \leftrightarrow (H_2CO_3) \leftrightarrow H^+ + HCO_3^- \quad (6)$$

$$HCO_3^- \leftrightarrow H^+ + CO_3^{2-} \quad (7)$$

It is interesting to point out that all products obtained in the photoreduction of $CO_2$ were derived from $CO_2^-$ radical and not from $CO_3^{2-}$ and $HCO_3^-$. No precipitation of $Na_2CO_3$ or $NaHCO_3$ was observed in all the tests, including the blank tests. According to Yoo et al. [54], the precipitation of those species occurs at higher NaOH concentrations, above 4–5% (w/w). In order to evaluate the efficiency in absorbing photons and generating products, the quantum yields were calculated for all the photocatalysts and are shown in Table 4.

Quantum yield calculation involves variables such as external area of the photoreactor, irradiation time and amount of photons absorbed by the photocatalyst. The variables involved had the same value for all the photocatalysts. Only the amount of absorbed photons, the amount of obtained product and the number of electrons had modifications. The amount of absorbed photons did not show great variation between the photocatalysts. This does not directly indicate that one photocatalyst will be less or more efficient than another, because the ability to absorb photons is not related to the ability to keep the electron-hole pair photoactive. Therefore, the quantum yield results presented the variation related to the amount of product.

**Table 4**
Quantum yields of $CH_4$ and CO production after 24 hour-irradiation.

| Materials | $\Phi_{CH4}$ (%) | $\Phi_{CO}$ (%) | $\Phi_T$ |
|---|---|---|---|
| $TiO_2$ (P-25) | 0.48 | 2.07 | 2.56 |
| $TiO_2$ | 0.49 | 1.37 | 1.86 |
| CT | 0.59 | 1.56 | 2.15 |
| CZT | 0.70 | 1.45 | 2.16 |

Values between 0.48 and 0.70% were obtained for $CH_4$ formation and are consistent with the literature [28,55]. Li et al. [27] found 0.85% and 0.56% for CO and $CH_4$, respectively; and total quantum yield was 1.41%. As can be seen, CT and CZT grew 20 and 44%, respectively, in the quantum yield for $CH_4$ in comparison with $TiO_2$ and $TiO_2$ (P-25). CT and CZT photocatalysts showed similar total quantum yield. However, CZT was more efficient for the production of $CH_4$. Despite the fact that $TiO_2$ (P-25) showed the highest $\Phi_T$, this result was mainly due to the highest efficiency on CO formation. This means that the commercial photocatalyst presented lower performance if compared to the prepared photocatalysts in the conversion of CO to $CH_4$.

## 4. Conclusion

The physicochemical characterization has shown that copper oxide is found dispersed on $TiO_2$ independent of the preparation method, co-precipitation or impregnation. Co-precipitation deposition caused the formation of filamentous structures on CZT surface, in which the zincite phase (ZnO) has been identified. Addition of copper and zinc oxides to $TiO_2$ has promoted a decrease in specific area if compared to pure $TiO_2$. DRS UV–vis spectra have indicated that CZT photocatalyst increases the photocatalytic activity if compared to the other materials. The TPD-$CO_2$ results revealed that both CT and CZT samples have $CO_2$ stronger interaction than that evidenced on pure $TiO_2$. Besides, the amount of $CO_2$ chemisorbed/desorbed on CZT was higher, indicating a higher number of interaction sites.

Concerning the performance tests, all synthesized materials are active as photocatalysts aiming at $CH_4$ formation. The photocatalytic activity increased in the following order: $TiO_2$ (P-25) ~ $TiO_2$ < CT < CZT, with $CH_4$ production in the range from 126 to 184 $\mu mol/g_{cat}$. It can be pointed out that the strength and amount of $CO_2$ adsorption sites have influenced the products formed in the photocatalytic reaction studied. Regarding to the liquid products, the presence of both cations $Cu^{2+}$ and $Cu^{1+}$ promoters in the photocatalysts was responsible for the lack of $CH_3OH$ production. Similar amounts of $CH_4$ produced using prepared $TiO_2$ and commercial $TiO_2$ (P-25, Degussa) suggest that the crystalline brookite phase has good activity in photocatalysis. Finally, the high photoactivity presented by Cu–Zn based photocatalysts in relation to reference P-25 (Degussa) is a guarantee that these materials are efficient photocatalysts with potential use in the photoreduction of $CO_2$ with $H_2O$.

## Acknowledgments

The authors would like to thank the National Council for Scientific and Technological Development (CNPq) for financial support. The authors also thank M.Sc. Carlos André C. Perez (NUCAT), Dr. Fábio Barboza Passos and M.Sc. Hugo A. Oliveira (RECAT/Universidade Federal Fluminense) for XPS analyses.

## References

[1] Q. Schiermeier, Nature 470 (2011) 316.
[2] C. Azar, H. Rodhe, Science 276 (1997) 1818–1819, http://www.sciencedirect.com/science/article/pii/S0167299106818495.
[3] G.I. Pearman, D. Etheridge, F. de Silva, P.J. Fraser, Nature 320 (1986) 248–250.
[4] H. Herzog, Energ. Econ. 33 (2011) 597–604.
[5] P.D. Tran, L.H. Wong, J. Barber, J.S.C. Loo, Energy Environ. Sci. 5 (2012) 5902–5918.
[6] J. Schneider, H. Ji, J.T. Muckermana, E. Fujita, Chem. Soc. Rev. 41 (2012) 2036–2051.
[7] S.S. Tan, L. Zou, E. Hu, Catal. Today 115 (2006) 269–273.
[8] S. Xu, D.D. Sun, Int. J. Hydrog. Energy 34 (2009) 6096–6104.
[9] L.S. Yoong, F.K. Chong, B.K. Dutta, Energy 34 (2009) 1652–1661.
[10] G. Guan, T. Kida, T. Harada, M. Isayama, A. Yoshida, Appl. Catal. A 249 (2003) 11–18.
[11] B. Kumari, S. Sharma, N. Singh, A. Verma, V.R. Satsangi, S. Dass, R. Shrivastav, Int. J. Hydrog. Energy 39 (2014) 18216–18229.
[12] G. Mahmodi, S. Sharifnia, F. Rahimpour, S.N. Hosseini, Sol. Energy Mater. Sol. Cells 111 (2013) 31–40.
[13] L. Liu, Y. Li, Air Qual. Res. 14 (2014) 453–469.
[14] D. Li, H. Haneda, J. Photochem. Photobiol. A 155 (2003) 171–178.
[15] H.W. Slamet, E. Nasution, S. Purnama, J. Kosela, Gunlazuardi, Catal. Commun. 6 (2005) 313–319.
[16] M. Watanabe, Surf. Sci. Lett. 279 (1992) 236–242.
[17] A. Pérez-Larios, R. Lopez, A. Hernández-Gordillo, F. Tzompantzi, R. Gómez, L.M. Torres-Guerra, Fuel 100 (2012) 139–143.
[18] M.M. Rodriguez, X.H. Peng, L.J. Liu, Y. Li, J.M. Andino, J. Phys. Chem. C 116 (2012) 19755–19764.
[19] K. Kočí, L. Obalová, Z. Lacný, Chem. Pap. 62 (2008) 1–9.
[20] D. Luo, Y. Bi, W. Kan, N. Zhang, S. Hong, J. Mol. Struct. 994 (2011) 325–331.
[21] Q. Zhang, Y. Li, E.A. Ackerman, M. Gajdardziska-Josifovska, H. Li, Appl. Catal. A 400 (2011) 195–202.
[22] M. Pelaez, A.A. De La Cruz, E. Stathatos, P. Falaras, D.D. Dionysiou, Catal. Today 144 (2009) 19–25.
[23] M. Hamadanian, A. Reisi-Vanani, A. Majedi, Mater. Chem. Phys. 116 (2009) 376–382.
[24] L. Zhou, J. Deng, Y. Zhao, W. Liu, L. An, F. Chen, Mater. Chem. Phys. 117 (2009) 522–527.
[25] S.U.M. Khan, M. Al-Shahry, W.B. Ingler, Science 297 (2002) 2243–2245.
[26] G.S. Wu, J.L. Wen, J.P. Wang, D.F. Thomas, A.C. Chen, Mater. Lett. 64 (2010) 1728–1731.
[27] Y. Li, W.-N. Wang, Z. Zhan, M.-H. Woo, C.-Y. Wu, P. Biswas, Appl. Catal. B 100 (2010) 386–392.
[28] I.-H. Tseng, W.-C. Chang, J.C.S. Wu, Appl. Catal. B 37 (2002) 37–48.
[29] N.S. Resende, J.-G. Eon, M. Schmal, Preparation of Catalysts VI: Scientific Bases for the Preparation of Heterogeneous Catalysts, vol. 91, 1995, pp. 1059–1067.
[30] M. Behrens, J. Catal. 267 (2009) 24–29.
[31] K. Kočí, L. Obalová, L. Matějová, D. Plachá, Z. Lacný, J. Jirkovský, O. Šolcová, Appl. Catal. B 89 (2009) 494–502.
[32] K.-H. Kim, S.-K. Ihm, J. Hazard. Mater. 146 (2007) 610–616.
[33] C. Shifu, Z. Wei, Z. Sujuan, L. Wei, Chem. Eng. J. 148 (2009) 263–269.
[34] D.V. César, R.F. Robertson, N.S. Resende, Catal. Today 133 (2008) 136–141.
[35] S. Xu, J. Ng, X. Zhang, H. Bai, D.D. Sun, Int. J. Hydrog. Energy 35 (2010) 5254–5261.
[36] I.-H. Tseng, J.C.S. Wu, H.-Y. Chou, J. Catal. 221 (2004) 432–440.
[37] J. Papavasiliou, G. Avgouropoulos, T. Ioannides, Appl. Catal. B 66 (2006) 168–174.
[38] H. Zhu, M. Shen, Y. Kong, J. Hong, Y. Hu, T. Liu, L. Donga, Y. Chen, C. Jian, Z. Liu, J. Mol. Catal. A: Chem. 219 (2004) 155–164.
[39] K.G. Chanchlani, R.R. Hudgins, P.L. Silveston, J. Catal. 136 (1992) 59–75.
[40] G. Colón, M. Maicu, M.C. Hidalgo, J.A. Navio, Appl. Catal. B 67 (2006) 41–51.
[41] S. Li, Z. Ma, J. Zhang, Y. Wu, Y. Gong, Catal. Today 139 (2008) 109–112.
[42] W. Choi, Catal. Surv. Asia 10 (2006) 16–28.
[43] F. Arena, G. Italiano, K. Barbera, S. Bordiga, G. Bonura, L. Spadaro, F. Frusteri, Appl. Catal. A 350 (2008) 16–23.
[44] T.I. Ozawa, M. Wasai, H. Tada, et al., J. Colloid Interface Sci. 281 (2005) 510–513.
[45] S.L. Isley, E.R. Anderson, R.L. Penn, Influence of ionic strength on brookite content in sol–gel synthesized titania before and after hydrothermal aging, in: Nanostructured Metal Oxides: Processing and Applications, The Electrochemical Society, Pennington, 2006, pp. 37–46.
[46] P.L. Richardson, M.L.N. Perdigoto, W. Wang, R.J.G. Lopes, Appl. Catal. B 126 (2012) 200–207.
[47] L. Matějová, K. Kočí, M. Reli, L. Čapek, V. Matějka, O. Šolcová, L. Obalová, Appl. Surf. Sci. 285 (2013) 688–696.
[48] T. Yui, A. Kan, C. Saitoh, K. Koike, T. Ibusuki, O. Ishitani, Appl. Mater. Interfaces 3 (2011) 2594–2600.
[49] Q.-H. Zhang, W.-D. Han, Y.-L. Hong, J.-G. Yu, Catal. Today 148 (2009) 335–340.
[50] C.-C. Lo, C.-H. Hung, C.-S. Yuan, Y.-L. Hung, Chin. J. Catal. 28 (2007) 528–534.
[51] M. Matsuoka, M. Kitano, M. Takeuchi, K. Tsujimaru, M. Anpo, J.M. Thomas, Catal. Today 122 (2007) 51–61.
[52] L. Liu, C. Zhao, Y. Li, J. Phys. Chem. C 116 (2012) 7904–7912.
[53] G.R. Dey, A.D. Belapurkar, K. Kishore, J. Photochem. Photobiol. A 163 (2004) 503–508.
[54] M. Yoo, S.-Jun Han, J.-Ho Wee, J. Environ. Manage. 114 (2013) 512–519.
[55] K. Ikeue, S. Nozaki, M. Ogawa, M. Anpo, Catal. Today 74 (2002) 241–248.